Supporting Information

Spin state modulation and chiral hierarchical assembly via amine-driven single-crystal-to-single-crystal transformation

Xu Ying,[a] Zhenhua Zhu,*[a] Peng Xu,[a, b] Quan Zhou,[a, b] and Jinkui Tang*[a, b]

[a] State Key Laboratory of Rare Earth Resource Utilization, Changchun Institute of Applied Chemistry, Chinese Academy of Sciences, Changchun 130022, P. R. China.

[b] School of Applied Chemistry and Engineering, University of Science and Technology of China, Hefei 230026, P. R. China

Table of Contents

1. Experimental Procedures

Materials and Synthesis. The starting materials were purchased from commercially available sources. ^{1}H NMR measurements were carried out on Bruker AV400 MHz spectrometer. Chemical shifts are expressed in δ units (ppm) with the residual solvent peak (δH = 2.50 ppm for $((CD_3)_2SO$, δH = 3.31 ppm for CD_3OD). Fourier transform infrared (FTIR) data were collected on a Nicolet 6700 Flex FTIR spectrometer in the range from 4000 to 550 cm^{-1}, which is equipped with a smart iTR attenuated total reflectance (ATR) sampling accessory.

Synthesis of H_2L

4-iodo-2,6-di(1*H*-imidazole-2-yl)pyridine (**H_2L**) was synthesized according to the published methods[1, 2]. ^{1}H NMR (400 MHz, $(CD_3)_2SO$): δ 12.69 (s, 2H), 8.18 (s, 2H), 7.52 (s, 2H), 7.16 (s, 2H).

Synthesis of Fe-BF_4

A mixture of **H_2L** (67.4 mg, 0.2 mmol) and $Fe(BF_4)_2 \cdot 6H_2O$ (33.7 mg, 0.1 mmol) in CH_3CN (10 mL) was stirred for 5 h, and then this mixture was filtered. Dark-red block-shaped single crystals were obtained by slow diffusion of ether into the filtrate after two weeks. Yield: 48 mg, 53%. Elemental analysis (%) calcd for $[Fe(L)_2](BF_4)_2$: N, 15.50; H, 1.78; C, 29.24. Found: N, 15.00; H, 1.97; C, 29.73. IR (cm^{-1}): 3566(br), 3280(m), 3138(br), 2252(w), 1610(m), 1532(m), 1491(w), 1461(s), 1371(w), 1289(w), 1259(w), 1199(w), 1170(w), 1050(s), 1011(s), 989(s), 933(m), 854(m), 787(w), 779(w), 733(m), 665(m), 619(w), 584(w), 570(w), 561(w).

Synthesis of Fe-1H

The single crystals of **Fe-BF_4** (1eq, 22 mg) and and 3 eq of Et_3N (3 eq) were added in CH_3CN (3 mL). The system was left undisturbed at room temperature, and the crystals hardly dissolved at all. Black block-shaped single crystals were obtained after 3 days. Yield: 10 mg, 56%. Elemental analysis (%) calcd for [Fe(HL)(L)]: N, 19.26; H, 1.80; C, 36.34. Found: N, 19.08; H, 1.80; C, 36.87. IR (cm^{-1}): 3111(w), 3080(w), 2297(br), 1922(br), 1586(w), 1567(w), 1533(m), 1504(m), 1437(s), 1418(s), 1342(w), 1299(m), 1261(m), 1210(m), 1161(w), 1138(m), 1098(w), 1074(w),

997(m), 943(w), 922(w), 881(w), 862(w), 844(w), 836(w), 782(w), 768(m), 746(m), 703(w), 624(w), 588(w), 577(w), 564(w).

Synthesis of Fe-Et_3N

Fe-Et_3N was synthesized in a similar procedure as **Fe-1H** except that excess Et_3N (7 eq) was used, giving black block-shaped single crystals. Yield: 60%. Elemental analysis (%) calcd for $[Fe(L)_2]\cdot(Et_3NH)\cdot H_2O$: N, 18.21; H, 3.57; C, 39.74. Found: N, 18.45; H, 3.23; C, 40.07. IR (cm^{-1}): 3063(w), 2974(w), 2219(br), 1922(br), 1584(m), 1529(m), 1497(w), 1434(s), 1421(m), 1349(w), 1314(w), 1295(m), 1261(m), 1218(m), 1160(w), 1135(m), 1096(w), 1072(w), 1029(w), 1004(w), 941(w), 925(w), 870(w), 827(w), 792(m), 765(m), 754(w), 741(m), 706(m), 637(w), 604(w), 589(w), 578(w), 562(w).

Synthesis of Fe-*R*-QNO

Fe-*R*-QNO was synthesized in a similar procedure as **Fe-1H** except that Et_3N (3 eq) was replaced with *R*-quinuclidinol (7 eq), giving dark-green block-shaped single crystals. Yield: 42%. Elemental analysis (%) calcd for $[Fe(L)_2]\cdot$(*R*-QNO-H): N, 18.04; H, 3.07; C, 40.77. Found: N, 17.90; H, 2.93; C, 40.74. IR (cm^{-1}): 3069(w), 2928(w), 2882(w), 2157(br), 2027(br), 1587(m), 1534(s), 1502(w), 1428(s), 1338(w), 1297(w), 1262(m), 1217(m), 1161(w), 1148(m), 1138(m), 1080(w), 1036(w), 1002(w), 975(w), 959(w), 934(w), 923(w), 886(w), 863(w), 850(w), 834(w), 796(w), 773(m), 758(w), 745(s), 708(w), 628(w), 604(w), 589(w), 572(w), 563(w).

Synthesis of Fe-*S*-QNO

Fe-*S*-QNO was synthesized in a similar procedure as **Fe-1H** except that Et_3N (3 eq) was replaced with *S*-quinuclidinol (7 eq), giving dark-green block-shaped single crystals. Yield: 41%. Elemental analysis (%) calcd for $[Fe(L)_2]\cdot$(*S*-QNO-H): N, 18.04; H, 3.07; C, 40.77. Found: N, 17.59; H, 3.21; C, 40.69. IR (cm^{-1}): 3074(w), 2945(w), 2182(br), 1585(m), 1533(s), 1503(w), 1430(s), 1349(w), 1318(w), 1300(w), 1263(m), 1255(m), 1218(m), 1162(w), 1139(m), 1127(m), 1074(w), 1030(w), 1002(w), 986(w), 971(w), 931(w), 924(w), 869(w), 838(w), 796(w), 770(w), 755(w), 742(s), 709(w), 625(w), 588(w), 568(w).

2. X-ray Crystallography

Single-crystal X-ray diffraction were measured by using a Bruker SMART APEX diffractometer with graphite-monochromatized Mo Kα radiation (λ = 0.71073 Å). The structures were solved by Intrinsic Phasing using SHELXT and refined by Least Squares minimization using SHELXL in OLEX2[3-5]. Non-hydrogen atoms in crystals were refined anisotropically. Hydrogen atoms were constrained to calculated positions and refined using the riding model. Crystallographic data can be obtained free of charge from the Cambridge Crystallographic Data Centre via www.ccdc.cam.ac.uk/data_request/cif and the deposition numbers of these data are listed in Table S1, S4, S7 and S10. Crystallographic data, selected bond distances and bond angles are presented in table S1 to S12.

Table S1. Crystal data and structure refinement for **Fe-BF$_4$**.

Compound	**Fe-BF$_4$ (300 K)**	**Fe-BF$_4$ (400 K)**
Chemical formula	$C_{22}H_{16}B_2FeI_2N_{10}F_8$	$C_{22}H_{16}B_2FeI_2N_{10}F_8$
Formula weight	903.72	903.72
Crystal system	Orthorhombic	Orthorhombic
a (Å)	17.0583(7)	17.473(4)
b (Å)	10.2981(5)	10.057(3)
c (Å)	16.7884(8)	17.232(4)
α (°)	90.00	90.00
β (°)	90.00	90.00
γ (°)	90.00	90.00
V (Å^3)	2949.2(2)	3028.1(13)
Temperature (K)	300.0	400.0
Space group	*P*bcn	*P*bcn
Z	4	4
ρ_{calc} (g/cm^3)	2.035	1.982
F (000)	1728.0	1728.0
Radiation	MoKα	MoKα
Reflections collected	19836	12647
Independent reflns	2581	2709
R_{int}	0.0588	0.1663
GOF on F^2	1.039	1.024
R_1 (I ≥2 σ (*I*))	0.0404	0.0721
wR_2 (all data)	0.1062	0.1407
CCDC Number	2378478	2378488

Table S2. Selected bond distances (Å), intermolecular interactions (Å) and calculated distortion parameters (º) for **Fe-BF$_4$**.

Fe-BF$_4$ (300 K)		**Fe-BF$_4$ (400 K)**	
Fe1−N1	1.988(4)	Fe1−N1	2.133(10)
Fe1−N2	1.999(4)	Fe1−N2	2.138(10)
Fe1−N3	1.925(4)	Fe1−N3	2.080(8)
Fe−N_{av}	1.971	Fe−N_{av}	2.117
N4−H···F2	2.781	N5−H···F1	2.977
N5−H···F3	2.933	N4−H···F3	2.782
ϕ /°	178.79°	ϕ /°	178.39
θ /°	88.01	θ /°	86.99
Σ /°	88.48	Σ /°	124.73
Θ /°	288.56	Θ /°	402.91

Table S3. Selected bond angles (º) for **Fe-BF$_4$**.

Fe-BF$_4$ (300 K)		**Fe-BF$_4$ (400 K)**	
N1−Fe1−N1^1	93.4(2)	N1−Fe1−N1^1	96.7(6)
N1−Fe1−N2^1	89.82(16)	N1−Fe1−N2^1	90.5(4)
N1−Fe1−N3^1	99.00(16)	N1−Fe1−N3^1	103.2(4)
N1−Fe1−N2	159.85(14)	N1−Fe1−N2	152.1(4)
N1−Fe1−N3	80.13(16)	N1−Fe1−N3	75.8(4)
N2−Fe1−N1^1	89.82(16)	N2−Fe1−N1^1	90.5(4)
N2−Fe1−N2^1	94.0(2)	N2−Fe1−N2^1	95.7(5)
N2−Fe1−N3^1	101.14(15)	N2−Fe1−N3^1	104.7(3)
N2−Fe1−N3	79.72(15)	N2−Fe1−N3	76.4(3)
N3−Fe1−N1^1	99.01(16)	N3−Fe1−N1^1	103.2(4)
N3−Fe1−N2^1	101.14(15)	N3−Fe1−N2^1	104.7(3)
N3−Fe1−N3^1	178.8(2)	N3−Fe1−N3^1	178.4(6)
N1^1−Fe1−N2^1	159.85(14)	N1^1−Fe1−N2^1	152.1(4)
N1^1−Fe1−N3^1	80.13(16)	N1^1−Fe1−N3^1	75.8(4)
N2^1−Fe1−N3^1	79.72(15)	N2^1−Fe1−N3^1	76.4(3)

Table S4. Crystal data and structure refinement for **Fe-1H** and **Fe-Et$_3$N**.

Compound	**Fe-1H**	**Fe-Et$_3$N**
Chemical formula	$C_{22}H_{13}FeI_2N_{10}$	$C_{28}H_{30}FeI_2N_{11}O$
Formula weight	727.07	846.28
Crystal system	Monoclinic	Monoclinic
a (Å)	12.4436(4)	14.7593(13)
b (Å)	12.2404(3)	12.8026(13)
c (Å)	16.7090(5)	17.5364(19)
α (°)	90.00	90.00
β (°)	109.0840(10)	100.631(3)
γ (°)	90.00	90.00
V (Å^3)	2405.15(12)	3256.8(6)
Temperature (K)	302.0	301.0
Space group	$P2_1/n$	$P2_1/c$
Z	4	4
ρ_{calc} (g/cm^3)	2.008	1.726
F (000)	1388.0	1660.0
Radiation	MoKα	MoKα
Reflections	23172	38415
Independent reflns	4160	5769
R_{int}	0.0392	0.1284
GOF on F^2	1.046	1.064
R_1 (I ≥2 σ (I))	0.0318	0.0796
wR_2 (all data)	0.0787	0.2260
CCDC Number	2378479	2378480

Table S5. Selected bond distances (Å), intermolecular interactions (Å) and calculated distortion parameters (º) for **Fe-1H** and **Fe-Et$_3$N**.

Fe-1H		**Fe-Et$_3$N**	
Fe1−N1	1.942(3)	Fe1−N1	1.944(9)
Fe1−N2	1.929(3)	Fe1−N2	1.946(9)
Fe1−N3	1.912(3)	Fe1−N3	1.915(8)
Fe1−N4	1.927(3)	Fe1−N4	1.929(9)
Fe1−N5	1.971(3)	Fe1−N5	1.924(9)
Fe1−N6	1.910(3)	Fe1−N6	1.909(8)
Fe−N_{av}	1.932	Fe−N_{av}	1.928
N10−H···N7	2.783	N11−H···N9	2.893
I1···N9	3.108	I1···N8	3.016
ϕ /°	179.00	ϕ /°	177.96
θ /°	89.45	θ /°	88.85
Σ /°	75.97	Σ /°	78.47
Θ /°	249.61	Θ /°	265.59

Table S6. Selected bond angles (º) for **Fe-1H** and **Fe-Et$_3$N**.

Fe-1H		**Fe-Et$_3$N**	
N1−Fe1−N2	162.51(13)	N1−Fe1−N2	162.3(4)
N1−Fe1−N3	81.21(12)	N1−Fe1−N3	81.5(4)
N1−Fe1−N4	91.53(13)	N1−Fe1−N4	89.4(4)
N1−Fe1−N5	91.28(13)	N1−Fe1−N5	93.1(4)
N1−Fe1−N6	97.99(13)	N1−Fe1−N6	99.8(3)
N2−Fe1−N3	81.34(12)	N2−Fe1−N3	81.0(4)
N2−Fe1−N4	92.48(13)	N2−Fe1−N4	92.0(4)
N2−Fe1−N5	90.10(13)	N2−Fe1−N5	91.1(4)
N2−Fe1−N6	99.45(13)	N2−Fe1−N6	97.8(3)
N3−Fe1−N4	99.10(12)	N3−Fe1−N4	101.4(4)
N3−Fe1−N5	98.76(12)	N3−Fe1−N5	96.8(4)
N3−Fe1−N6	179.02(13)	N3−Fe1−N6	177.9(4)
N4−Fe1−N5	162.14(13)	N4−Fe1−N5	161.7(3)
N4−Fe1−N6	81.47(12)	N4−Fe1−N6	80.2(4)
N5−Fe1−N6	80.67(13)	N5−Fe1−N6	81.5(4)

Table S7. Crystal data and structure refinement for **Fe-*R*-QNO** and **Fe-*S*-QNO**.

Compound	**Fe-*R*-QNO**	**Fe-*S*-QNO**
Chemical formula	$C_{35}H_{35}FeI_2N_{14}O$	$C_{35}H_{35}FeI_2N_{14}O$
Formula weight	977.42	977.42
Crystal system	Orthorhombic	Orthorhombic
a (Å)	12.4932(5)	12.5040(14)
b (Å)	14.0966(5)	14.0949(11)
c (Å)	22.0691(10)	22.028(2)
α (°)	90.00	90.00
β (°)	90.00	90.00
γ (°)	90.00	90.00
V (Å^3)	3886.6(3)	3882.2(6)
Temperature (K)	180.0	180.0
Space group	$P2_12_12_1$	$P2_12_12_1$
Z	4	4
ρ_{calc} (g/cm^3)	1.670	1.672
F (000)	1932.0	1932.0
Radiation	MoKα	MoKα
Reflections	26507	23451
Independent reflns	6875	6840
R_{int}	0.0721	0.1117
GOF on F^2	1.090	1.061
R_1 (I ≥2 σ (*I*))	0.0475	0.1175
wR_2 (all data)	0.1051	0.3124
CCDC Number	2378481	2468133

Table S8. Selected bond distances (Å) and intermolecular interactions (Å) for **Fe-*R*-QNO** and **Fe-*S*-QNO**.

Fe-*R*-QNO		**Fe-*S*-QNO**	
Fe1−N1	1.936(8)	Fe1−N1	1.917(2)
Fe1−N2	1.915(7)	Fe1−N2	1.915(2)
Fe1−N3	1.925(8)	Fe1−N3	1.959(2)
Fe1−N4	1.944(8)	Fe1−N4	1.933(2)
Fe1−N5	1.916(7)	Fe1−N5	1.916(2)
Fe1−N6	1.933(9)	Fe1−N6	1.923(2)
O1−H···N10	2.741	O1−H···N10	2.717
N11−H···N9	2.788	N11−H···N9	2.803
I1···N8	2.860	I1···N8	2.857

Table S9. Selected bond angles (º) for **Fe-*R*-QNO** and **Fe-*S*-QNO**.

Fe-*R*-QNO		**Fe-*S*-QNO**	
N1−Fe1−N2	81.9(3)	N1−Fe1−N2	81.7(8)
N1−Fe1−N3	162.6(3)	N1−Fe1−N3	162.3(8)
N1−Fe1−N4	91.8(4)	N1−Fe1−N4	90.3(9)
N1−Fe1−N5	98.8(3)	N1−Fe1−N5	99.2(8)
N1−Fe1−N6	90.7(4)	N1−Fe1−N6	91.0(9)
N2−Fe1−N3	80.8(3)	N2−Fe1−N3	80.6(8)
N2−Fe1−N4	98.9(4)	N2−Fe1−N4	98.5(8)
N2−Fe1−N5	179.3(4)	N2−Fe1−N5	178.8(8)
N2−Fe1−N6	98.4(4)	N2−Fe1−N6	98.4(8)
N3−Fe1−N4	92.0(3)	N3−Fe1−N4	91.9(8)
N3−Fe1−N5	98.5(3)	N3−Fe1−N5	98.5(8)
N3−Fe1−N6	90.6(4)	N3−Fe1−N6	92.0(8)
N4−Fe1−N5	81.2(3)	N4−Fe1−N5	80.7(8)
N4−Fe1−N6	162.7(3)	N4−Fe1−N6	163.0(8)
N5−Fe1−N6	81.5(3)	N5−Fe1−N6	82.4(8)

Table S10. Crystal data and structure refinement for **Fe-Re** obtained by the reduction of **Fe-Et$_3$N** with $NH_2OH{\cdot}HCl$ in MeOH.

Compound	**Fe-Re**
Chemical formula	$C_{22}H_{24}FeI_2N_{10}O_4Cl_2$
Formula weight	873.06
Crystal system	Triclinic
a (Å)	12.691(4)
b (Å)	13.266(4)
c (Å)	18.015(6)
α (°)	100.715(10)
β (°)	90.008(9)
γ (°)	118.477(9)
V (Å^3)	2605.5(14)
Temperature (K)	180.0
Space group	*P*1
Z	3
ρ_{calc} (g/cm^3)	1.669
F (000)	1272.0
Radiation	MoKα
Reflections	30278
Independent reflns	17086
R_{int}	0.2079
GOF on F^2	0.940
R_1 (I ≥2 σ (*I*))	0.0987
wR_2 (all data)	0.2186
CCDC Number	2468134

Table S11. Selected bond distances (Å) and intermolecular interactions (Å) for **Fe-Re** obtained by the reduction of **Fe-Et$_3$N** with $NH_2OH{\cdot}HCl$ in MeOH.

	Fe-Re				
Fe1−N1	1.96(3)	Fe1−N11	2.12(3)	Fe1−N21	1.97(3)
Fe1−N2	1.893(15)	Fe1−N12	2.105(19)	Fe1−N22	1.944(14)
Fe1−N3	2.01(3)	Fe1−N13	2.20(3)	Fe1−N23	1.93(3)
Fe1−N4	2.07(3)	Fe1−N14	2.17(3)	Fe1−N24	1.92(3)
Fe1−N5	1.921(15)	Fe1−N15	2.118(19)	Fe1−N25	1.840(15)
Fe1−N6	2.02(3)	Fe1−N16	2.13(3)	Fe1−N26	1.96(3)

Table S12. Selected bond angles (º) for **Fe-Re** obtained by the reduction of **Fe-Et$_3$N** with $NH_2OH{\cdot}HCl$ in MeOH.

	Fe-Re				
N1−Fe1−N2	79.7(10)	N11−Fe1−N12	76.0(11)	N21−Fe1−N22	81.0(10)
N1−Fe1−N3	160.0(11)	N11−Fe1−N13	149.1(13)	N21−Fe1−N23	162.2(12)
N1−Fe1−N4	92.5(13)	N11−Fe1−N14	92.6(14)	N21−Fe1−N24	89.5(12)
N1−Fe1−N5	99.9(11)	N11−Fe1−N15	111.2(11)	N21−Fe1−N25	99.7(11)
N1−Fe1−N6	91.3(13)	N11−Fe1−N16	97.5(13)	N21−Fe1−N26	93.7(13)
N2−Fe1−N3	80.5(10)	N12−Fe1−N13	73.1(12)	N22−Fe1−N23	81.2(11)
N2−Fe1−N4	99.5(11)	N12−Fe1−N14	98.6(13)	N22−Fe1−N24	97.8(10)
N2−Fe1−N5	177.9(11)	N12−Fe1−N15	170.6(10)	N22−Fe1−N25	178.9(11)
N2−Fe1−N6	97.6(10)	N12−Fe1−N16	110.2(12)	N22−Fe1−N26	98.6(10)
N3−Fe1−N4	93.0(13)	N13−Fe1−N14	91.3(15)	N23−Fe1−N24	91.9(13)
N3−Fe1−N5	99.9(10)	N13−Fe1−N15	99.4(13)	N23−Fe1−N25	98.1(11)
N3−Fe1−N6	89.0(12)	N13−Fe1−N16	93.8(13)	N23−Fe1−N26	90.0(13)
N4−Fe1−N5	82.7(11)	N14−Fe1−N15	75.5(13)	N24−Fe1−N25	81.5(10)
N4−Fe1−N6	162.9(11)	N14−Fe1−N16	151.0(15)	N24−Fe1−N26	163.6(11)
N5−Fe1−N6	80.3(10)	N15−Fe1−N16	75.5(12)	N25−Fe1−N26	82.1(10)

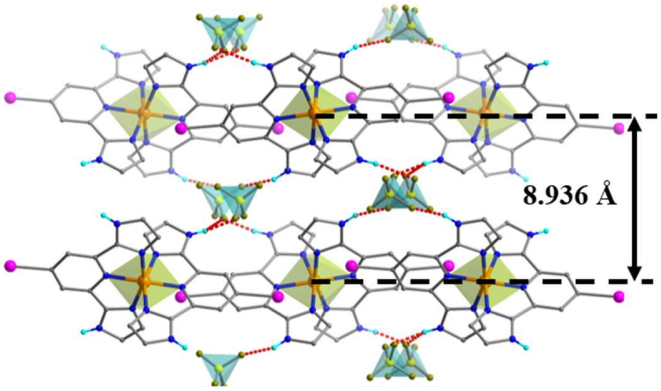

Figure S1. The packing diagram along the crystallographic *b* axis of **Fe-BF$_4$**. All hydrogen atoms except those involved in the H-bondings are omitted for clarity. Color modes: Fe(II) orange, N blue, C gray, I pink, B yellow, F dark yellow, H turquoise. Label: dash lines, N−H···F interactions.

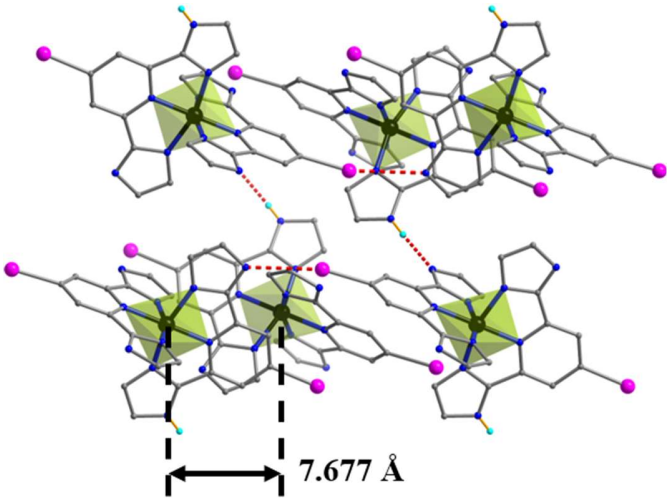

Figure S2. The packing diagram along the crystallographic *b* axis of **Fe-1H**. All hydrogen atoms except those involved in the H-bondings are omitted for clarity. Color modes: Fe(III) black, N blue, C gray, I pink, O red, H turquoise. Label: dash lines, N−H···N interactions.

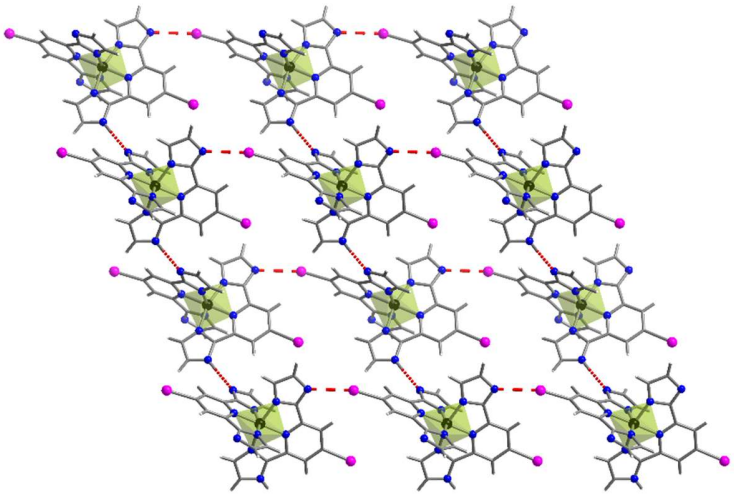

Figure S3. Supramolecular structures assembled by intermolecular non-covalent interactions in **Fe-1H**. All hydrogen atoms except those involved in the H-bondings are omitted for clarity. Color modes: Fe(III) black, N blue, C gray, I pink, O red, H turquoise. Label: dash lines, N−H···N and C−I···N interactions.

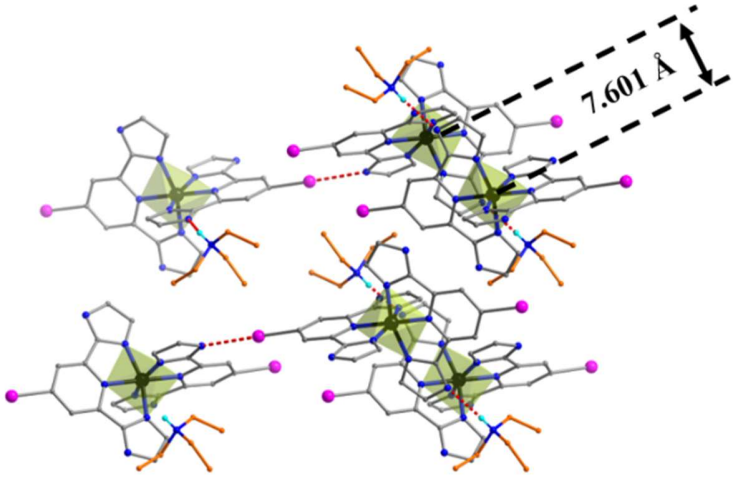

Figure S4. The packing diagram along the crystallographic *b* axis of **Fe-Et$_3$N**. Most H atoms and all solvents are omitted for clarity. Color modes: Fe(III) black, N blue, C in Fe(III) units gray, C in amines units orange, I pink, O red, H turquoise. Label: dash lines, hydrogen bonding interactions.

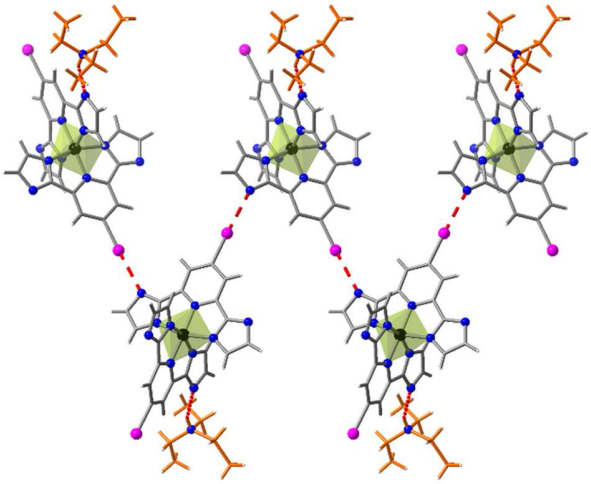

Figure S5. Supramolecular structures assembled by intermolecular non-covalent interactions in **Fe-Et$_3$N**. All hydrogen atoms except those involved in the H-bondings are omitted for clarity. Color modes: Fe(III) black, N blue, C in Fe(III) units gray, C in amines units orange, I pink, O red, H turquoise. Label: dash lines, N−H···N and C−I···N interactions.

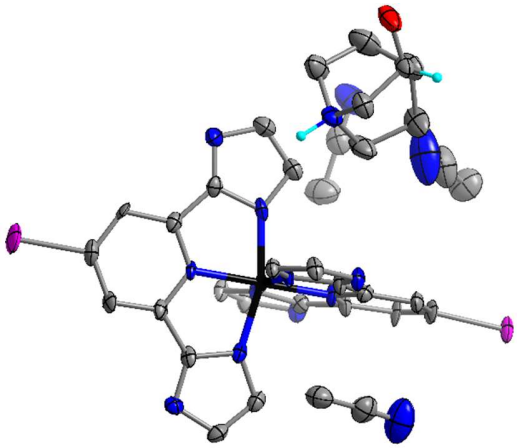

Figure S6. The asymmetric unit of **Fe-*R*-QNO**. Color modes: Fe(III) black, N blue, C gray, I pink, O red, H turquoise.

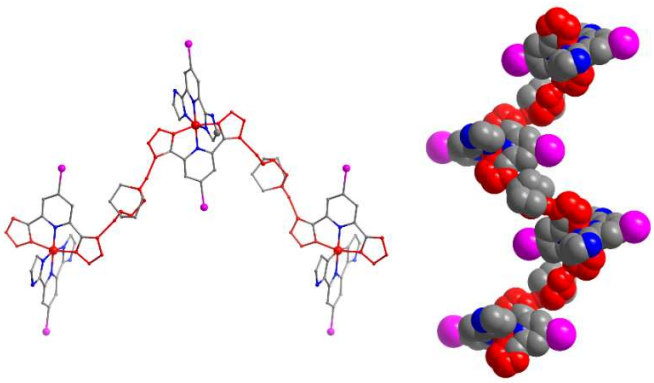

Figure S7. The hydrogen-bonded 1D helical chain of **Fe-*R*-QNO** with ball-and-stick (left) and space-filling model (right).

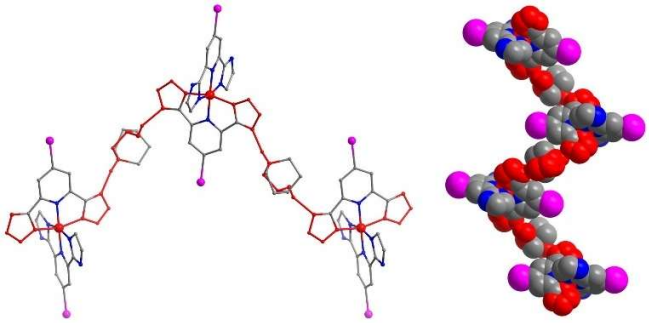

Figure S8. The hydrogen-bonded 1D helical chain of **Fe-*S*-QNO** with ball-and-stick (left) and space-filling model (right).

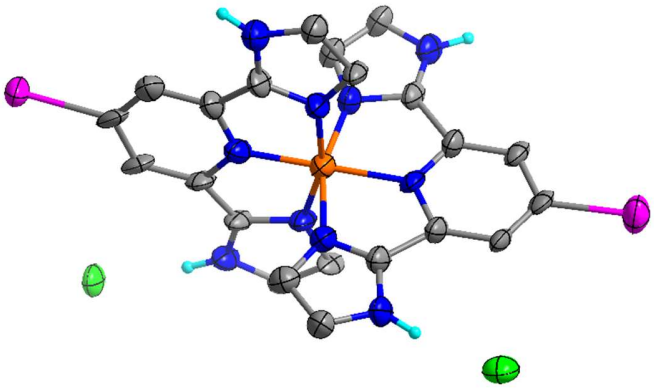

Figure S9. The crystal structure of **Fe-Re** obtained by the reduction of **Fe-Et_3N** with NH2OH·HCl in MeOH. Color modes: Fe(II) orange, N blue, C gray, I pink, O red, H turquoise.

3. Characterization and Magnetic Measurements

TGA data were recorded on Pyris Diamond TG/DTA analyzer. Ultraviolet-visible (UV-Vis) absorption spectra were collected on a Shimadzu UV-1750 in methanol. Circular dichroism (CD) measurements were performed on a JASCO J-1500 spectrometer using the KBr pellet method. The variable-temperature magnetization data was collected under a dc magnetic field of 1000 Oe in the temperature range 5-400 K on a Quantum Design MPMS-XL7 SQUID magnetometer equipped with a 7 T magnet. The experimental magnetic susceptibility data are corrected for the diamagnetism estimated from Pascal's tables and sample holder calibration[6]. X-band cw-EPR measurements were carried on a CIQTEK EPR200-Plus spectrometer.

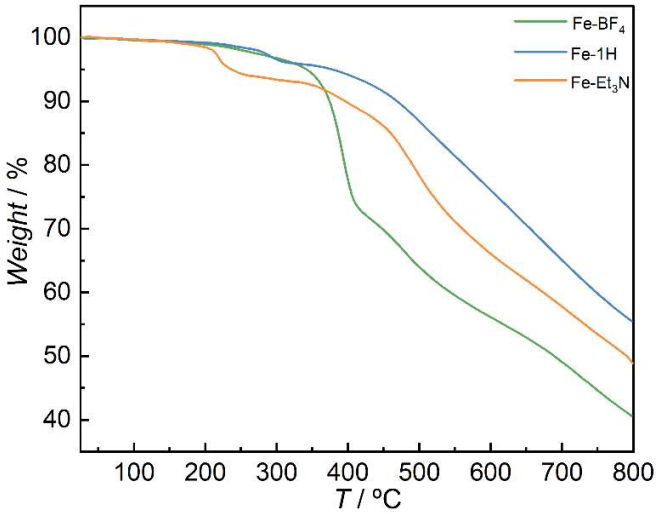

Figure S10. TGA data of **Fe-BF_4**, **Fe-1H** and **Fe-Et_3N**.

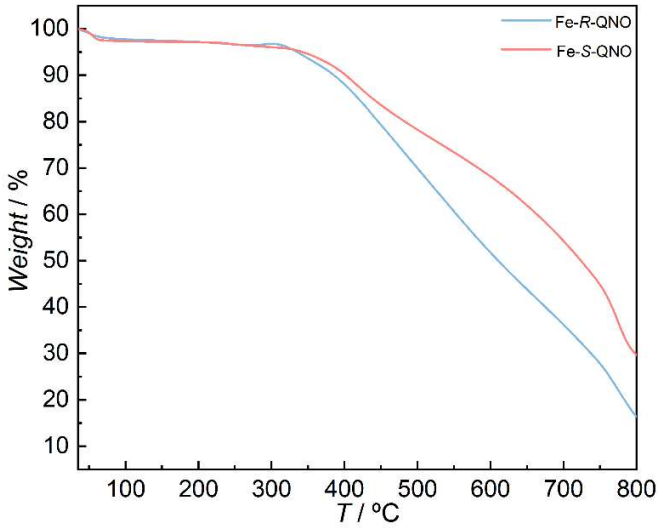

Figure S11. TGA data of **Fe-*R*-QNO** and **Fe-*S*-QNO**.

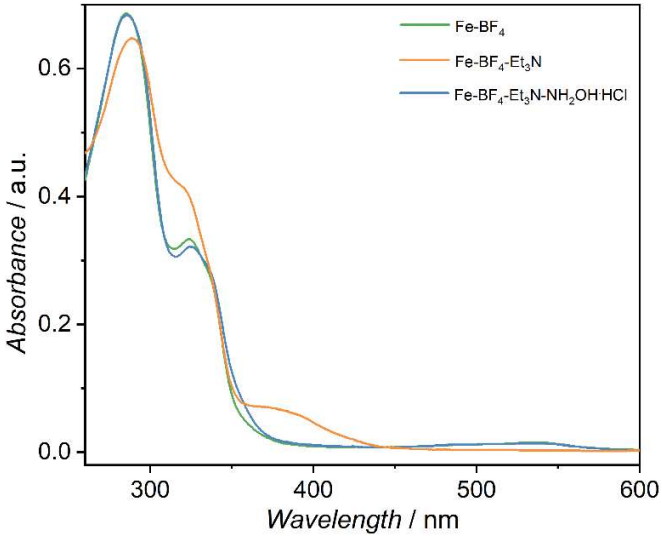

Figure S12. Changes in the UV-Vis absorption spectra of **Fe-BF4** (green) upon addition of Et_3N (orange) followed by NH2OH·HCl (blue) in MeOH (c = 10^{-5} M).

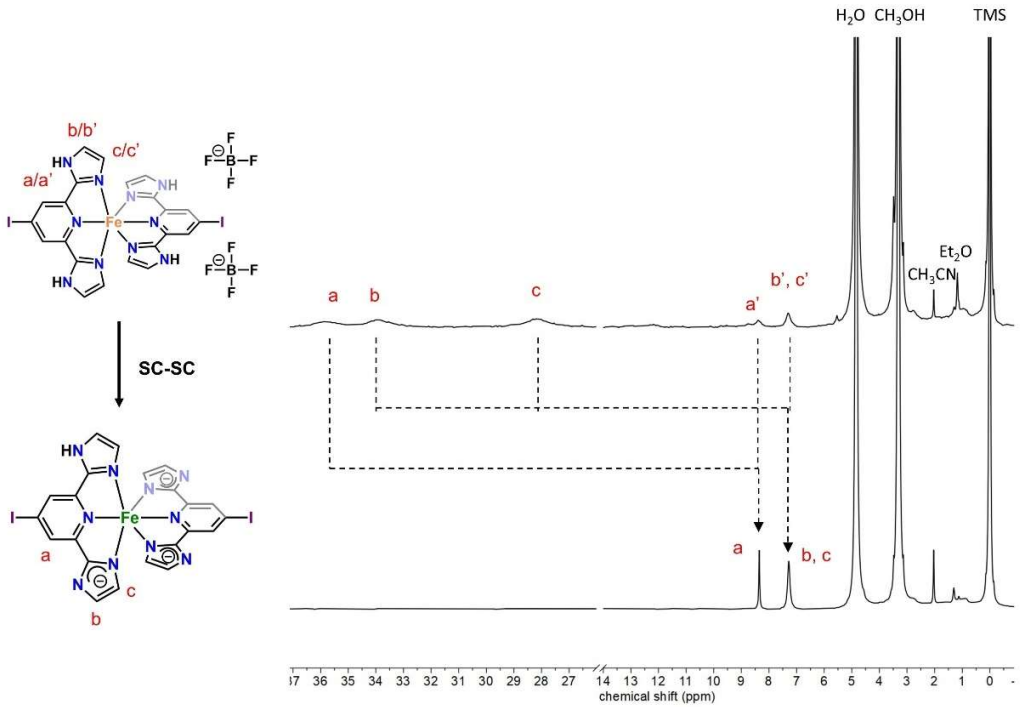

Figure S13. Changes in the ^{1}H NMR spectra during the SC–SC transformation from **Fe-BF$_4$** to **Fe-1H** in CD_3OD.

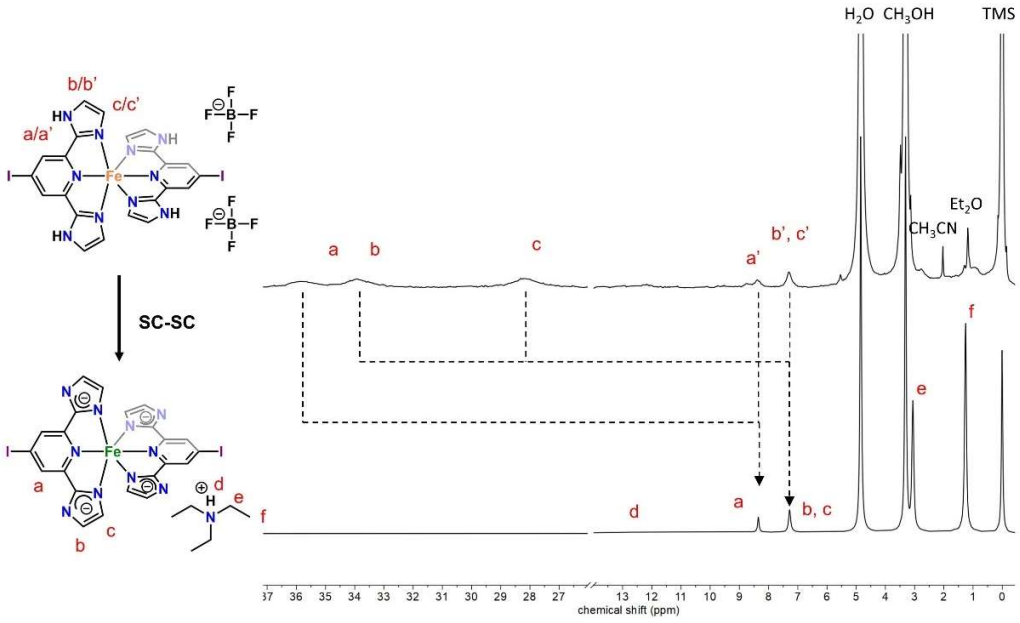

Figure S14. Changes in the ^{1}H NMR spectra during the SC–SC transformation from **Fe-BF$_4$** to **Fe-Et$_3$N** in CD_3OD.

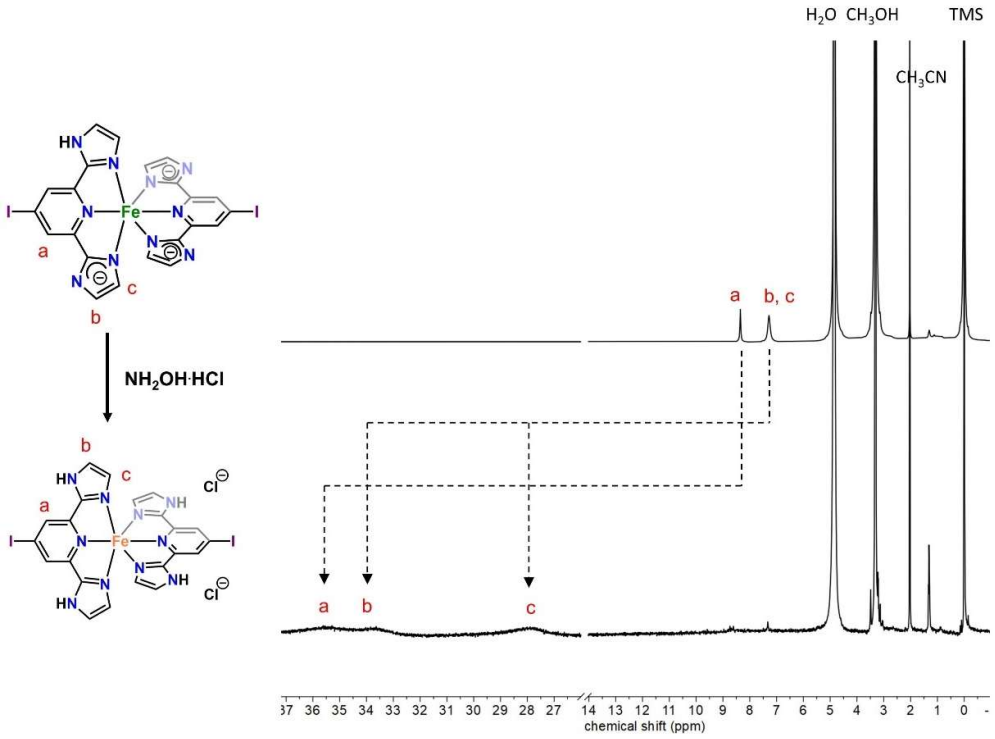

Figure S15. Changes in the ^{1}H NMR spectra of **Fe-1H** before and after reduction by $NH_2OH{\cdot}HCl$ in CD_3OD.

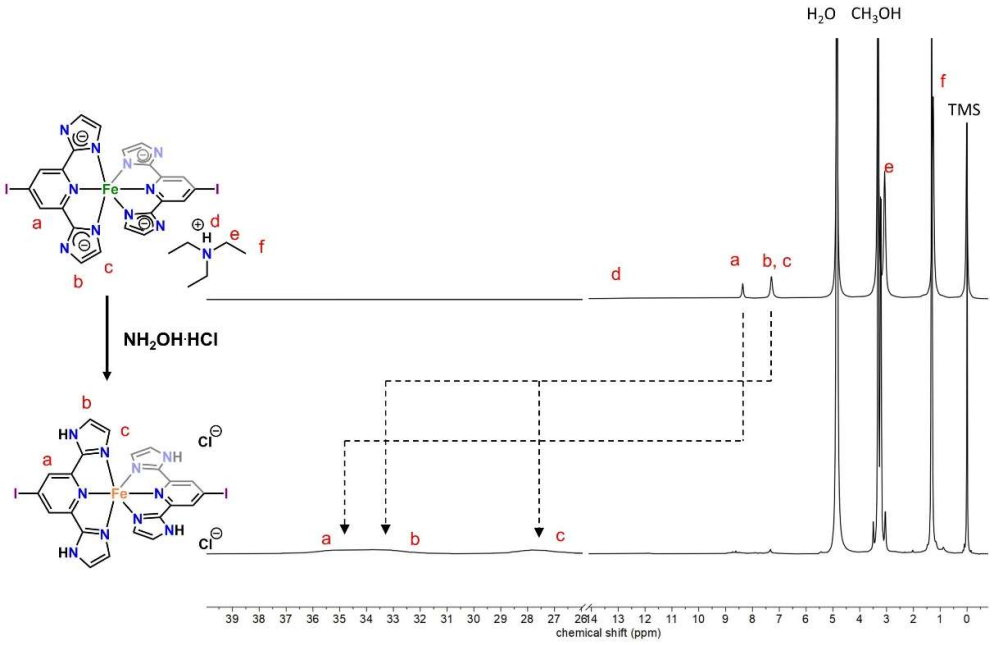

Figure S16. Changes in the ^{1}H NMR spectra of **Fe-Et$_3$N** before and after reduction by $NH_2OH{\cdot}HCl$ in CD_3OD.

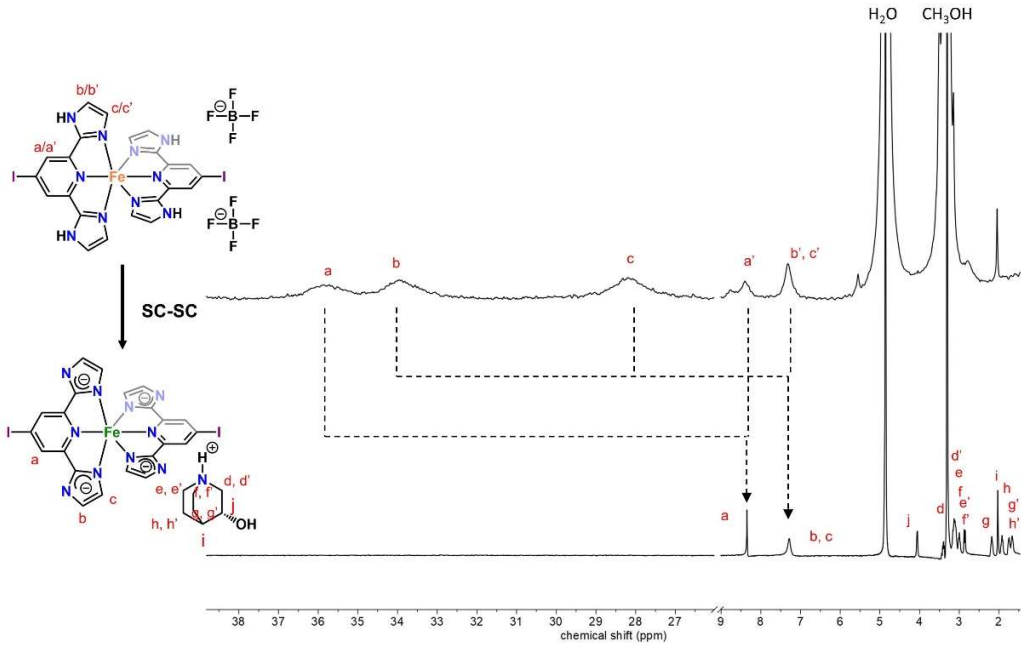

Figure S17. Changes in the ^{1}H NMR spectra during the SC–SC transformation from **Fe-BF$_4$** to **Fe-*R*-QNO** in CD_3OD.

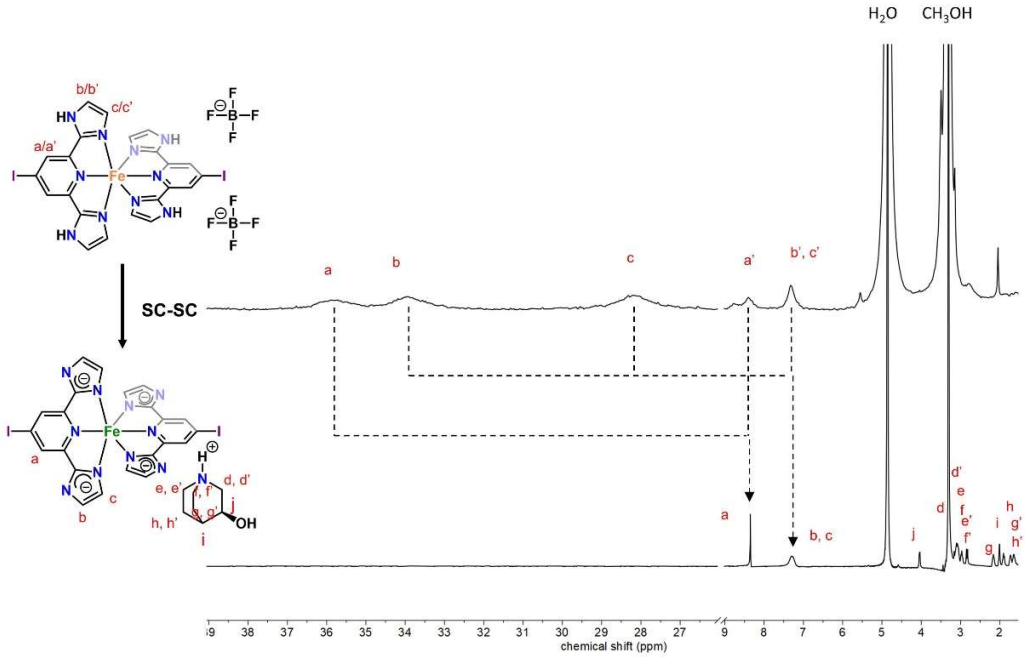

Figure S18. Changes in the ^{1}H NMR spectra during the SC–SC transformation from **Fe-BF$_4$** to **Fe-*S*-QNO** in CD_3OD.

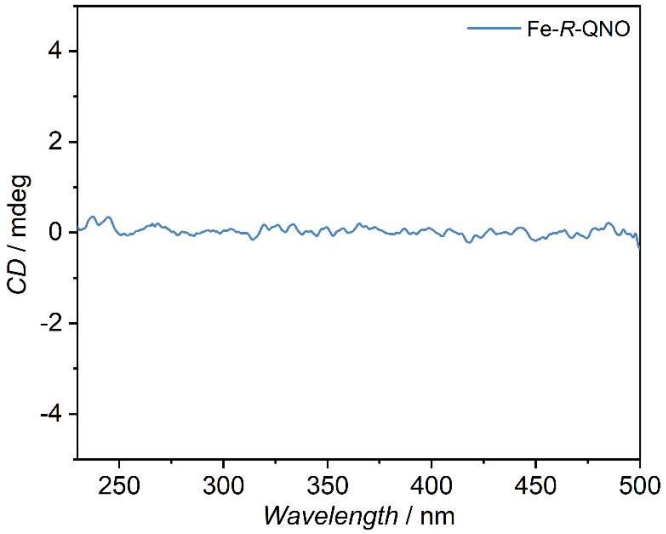

Figure S19. CD spectra of **Fe-*R*-QNO** in MeOH ($c = 10^{-5}$ M).

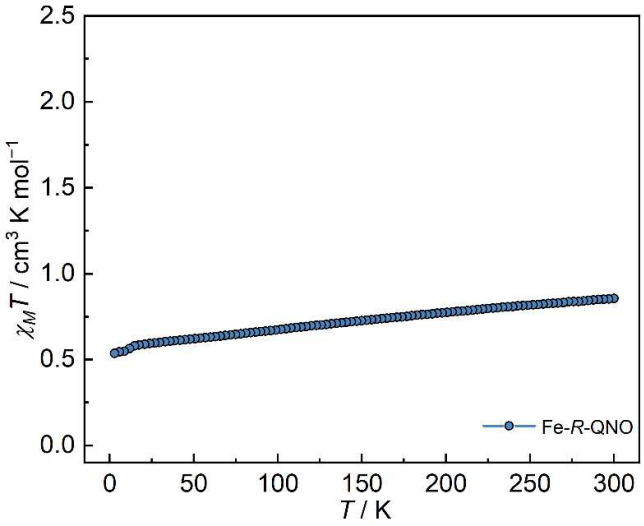

Figure S20. Temperature dependence of $\chi_M T$ values for **Fe-*R*-QNO**.

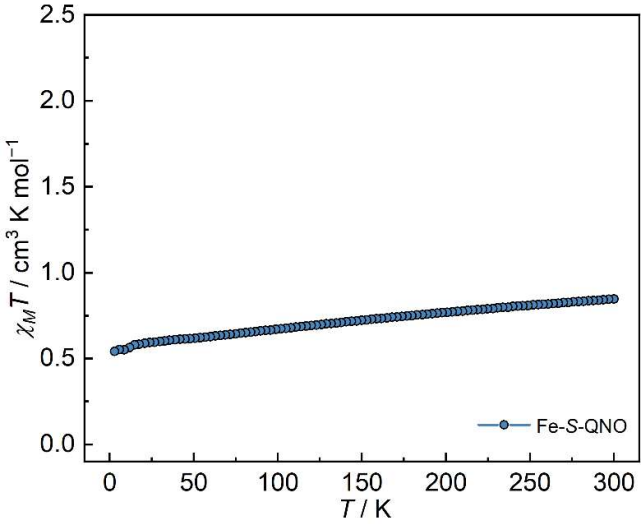

Figure S21. Temperature dependence of $\chi_M T$ values for **Fe-*S*-QNO**.

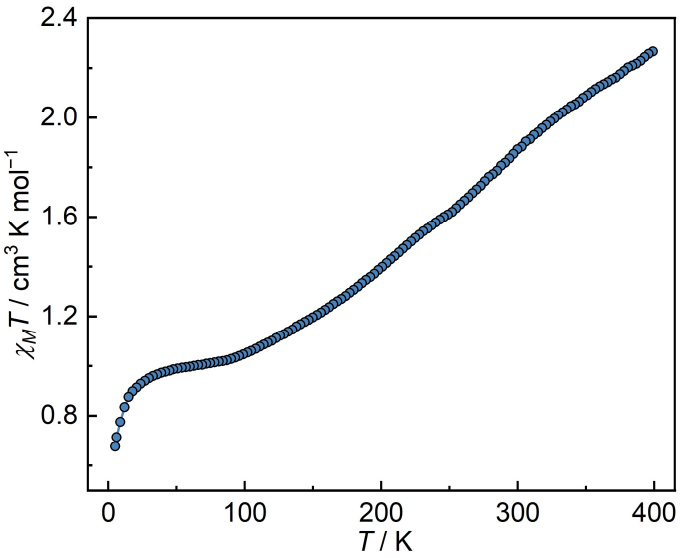

Figure S22. Temperature dependence of $\chi_M T$ values for **Fe-Re**.

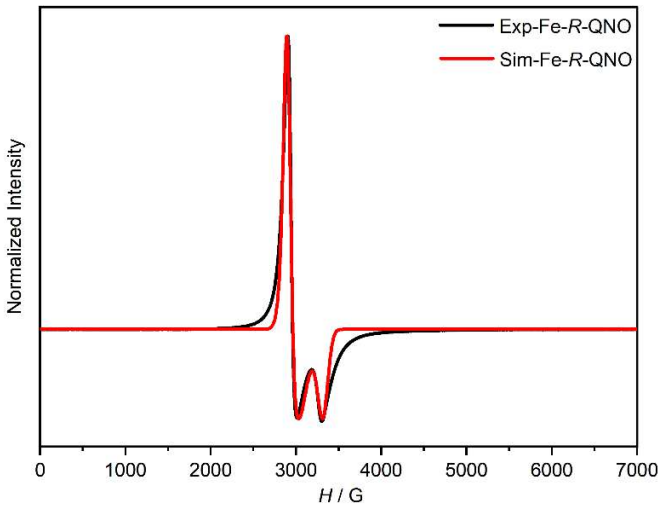

Figure S23. Experimental and simulated EPR spectra of **Fe-*R*-QNO** ($S = 1/2$, $g_x = 2.28$, $g_y = 2.25$, $g_z = 2.002$) at room temperature.

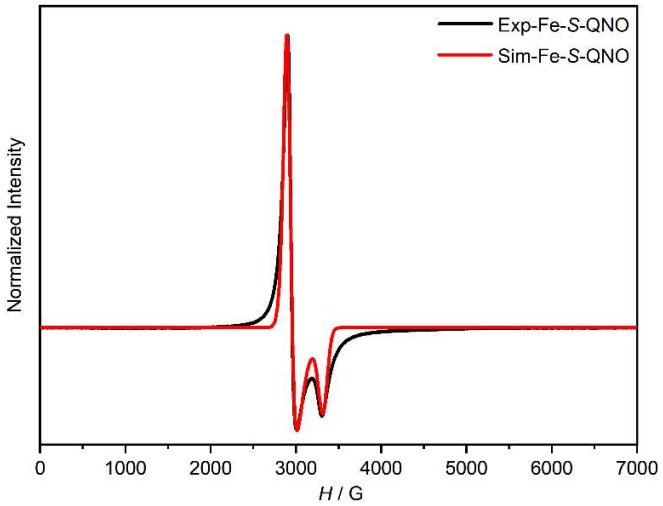

Figure S24. Experimental and simulated EPR spectra of **Fe-*S*-QNO** ($S = 1/2$, $g_x = 2.28$, $g_y = 2.26$, $g_z = 2.002$) at room temperature.

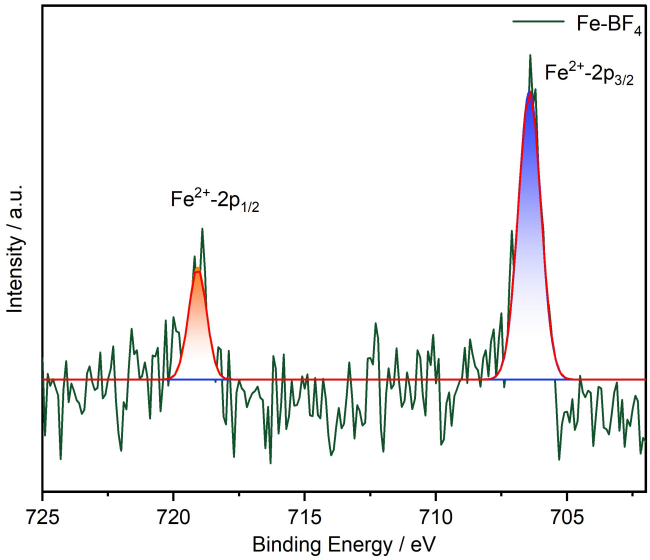

Figure S25. XPS spectra of the Fe 2p regions for **Fe-BF_4**.

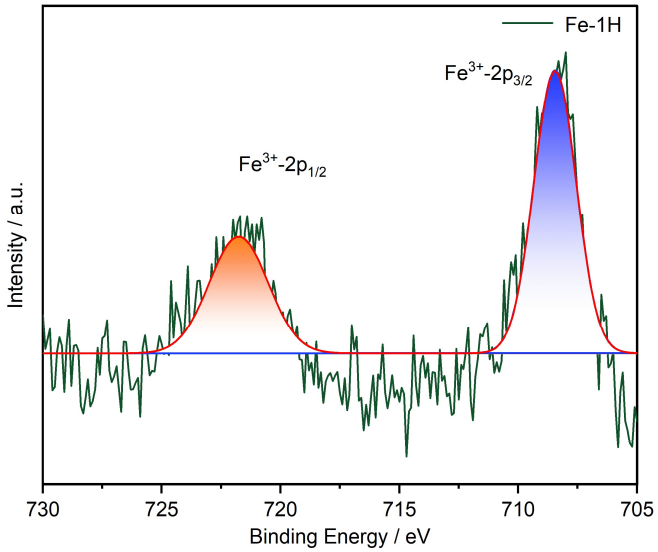

Figure S26. XPS spectra of the Fe 2p regions for **Fe-1H**.

4. References

1. B. G. Hashiguchi, K. J. Young, M. Yousufuddin, W. A. Goddard, III and R. A. Periana, Acceleration of nucleophilic CH activation by strongly basic solvents, *J. Am. Chem. Soc.*, 2010, **132**, 12542-12545.
2. S. Di Pietro, D. Imbert and M. Mazzanti, An efficient triazole-pyridine-bistetrazolate platform for highly luminescent lanthanide complexes, *Chem. Commun.*, 2014, **50**, 10323-10326.
3. O. V. Dolomanov, L. J. Bourhis, R. J. Gildea, J. A. K. Howard and H. Puschmann, *OLEX2*: a complete structure solution, refinement and analysis program, *J. Appl. Crystallogr.*, 2009, **42**, 339-341.
4. G. M. Sheldrick, Crystal structure refinement with *SHELXL*, *Acta. Crystallogr. C Struct. Chem.*, 2015, **71**, 3-8.
5. G. M. Sheldrick, *SHELXT* - integrated space-group and crystal-structure determination, *Acta. Crystallogr. A Found. Adv.*, 2015, **71**, 3-8.
6. E. A. Boudreaux and L. N. Mulay, *Theory and Applications of Molecular Paramagnetism*, John Wiley & Sons, New York, 1976.